JOURNAL OF combinatorial CHEMISTRY

Article

Scanning Raman Spectroscopy for Characterizing Compositionally Spread Films

A. Venimadhav, K. A. Yates, and M. G. Blamire

J. Comb. Chem., **2005**, 7 (1), 85-89• DOI: 10.1021/cc049927b • Publication Date (Web): 23 October 2004

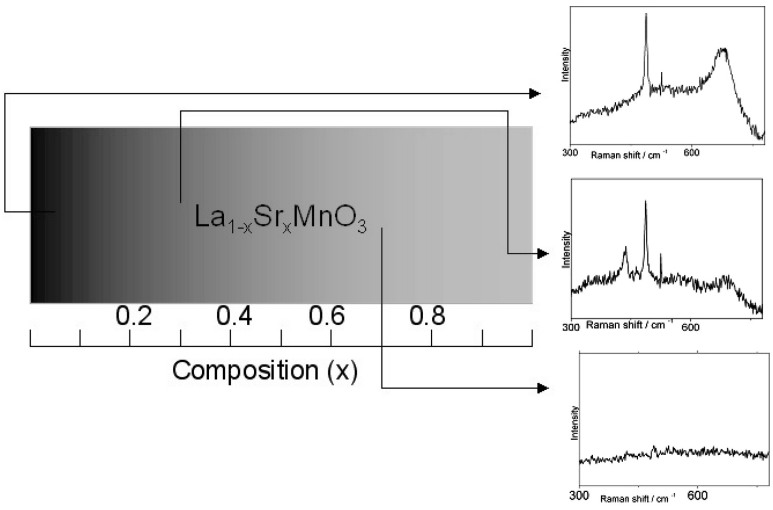

More About This Article

Additional resources and features associated with this article are available within the HTML version:

- Supporting Information
- Access to high resolution figures
- Links to articles and content related to this article
- Copyright permission to reproduce figures and/or text from this article

View the Full Text HTML

Journal of Combinatorial Chemistry is published by the American Chemical Society.
1155 Sixteenth Street N.W., Washington, DC 20036

Scanning Raman Spectroscopy for Characterizing Compositionally Spread Films

A. Venimadhav,* K. A. Yates, and M. G. Blamire

Department of Materials Science, University of Cambridge, Pembroke Street, Cambridge, CB2 3QZ, UK

Received March 31, 2004

Composition-spread $La_{1-x}Sr_xMnO_3$ thin films were prepared by pulsed laser deposition technique from $LaMnO_3$ and $SrMnO_3$ targets. The films were epitaxial with a continuous variation of the out-of-plane lattice parameter along the direction of composition gradient. Scanning Raman spectroscopy has been employed as a nondestructive tool to characterize the composition-spread films. Raman spectra showed the variation of the structural, Jahn Teller distortions and the presence of coexisting phases at particular compositions that are in agreement with the previous observation on the single-crystal samples. Raman spectra on the continuous composition-spread film also reveal the effect of disorder and strain on the compositions.

Introduction

Perovskite oxides with strong electron correlation exhibit very complex phase diagrams. The doped lanthanum manganites, in particular, display a variety of phases, including colossal magnetoresistance, charge-ordering at definite doping levels, and evidence for the coexistence of different phases at a given composition.[1] The Zener double exchange mechanism and the electron lattice coupling due to the Jahn Teller (JT) effect together control the transport and optical properties of these materials.[2] There is an increasing technological interest in the optimally doped regions of the phase diagram where these materials exhibit 100% spin polarization due to the development of a half-metallic ground state.[3] Finding the critical doping and phase boundaries from conventional preparation methods is laborious and rather time-consuming. For getting an overview of the entire composition of the inorganic materials, Briceño et al. have employed the combinatorial process.[4] Continuous variation of manganite compositions in thin film form has been created by combinatorial pulsed laser deposition systems.[5,6]

It is difficult to characterize compositionally spread films fully by nondestructive techniques, particularly evaluating stoichiometry and the analysis of impurity phases. Raman spectroscopy can be an ideal tool to find any impurities at micrometer levels and may be more efficient than X-ray diffraction and energy-dispersive analysis techniques.[7] Additionally, it provides information about the electronic and lattice processes responsible for the physical behavior of the material. Raman spectroscopy has proven to be a very useful technique for evaluating the oxygen stoichiometry[8] and cation disorder[9] in $YBa_2Cu_3O_{7-\delta}$, thereby helping in understanding of the relationship between the superconducting T_c and the crystal structure. It has also provided essential information about the lattice and JT distortion and orbital ordering in the manganites that occurs at variable doping levels.[10−20] In this paper, we demonstrate that the scanning Raman spectroscopic technique is an efficient tool for characterizing the continuous composition spread (CCS) film.

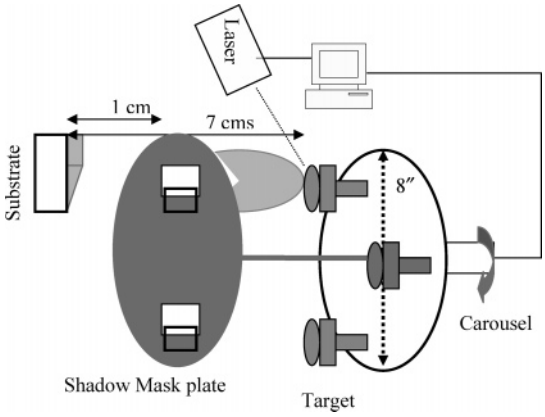

Figure 1. Combinatorial PLD setup.

Experiment

CCS films were deposited by the pulsed laser deposition (PLD) technique. Briceño et al. employed postannealing conditions for the films deposited at the ambient temperature.[4] Christen et al. obtained epitaxial continuous phases of perovskite oxides at the optimal growth conditions, there by avoiding extensive postannealing steps.[21] In this study, continuous-spread $(LaSr)MnO_3$ films have been prepared by sequential deposition of submonolayers from $LaMnO_3$ (LMO) and $SrMnO_3$ (SMO) targets using a multitarget carousel. The laser plume and the substrate were stationary during the complete deposition process. Composition variation is usually achieved by creating a thickness gradient of the constituent target materials on the substrate by manipulating the laser plume using shutters or moving masks. In our setup, we used a shadow mask plate with specific openings that mask the laser plume for different targets, as shown in the Figure 1. This plate is an extension to the target carousel placed at a distance 1 cm above the substrate.

* To whom correspondence should be addressed. E-mail: avm24@cus.cam.ac.uk.

10.1021/cc049927b CCC: $30.25
Published on Web 10/23/2004

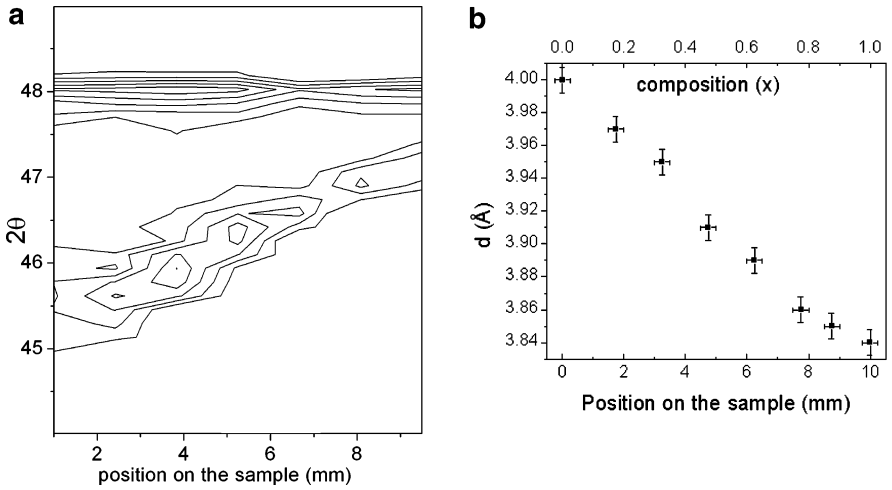

Figure 2. Intensity contour map constructed from $\theta-2\theta$ scans collected at 1.5-mm intervals along the sample. The actual *d* value measured at different positions is shown in the inset, with the intended composition on the upper panel.

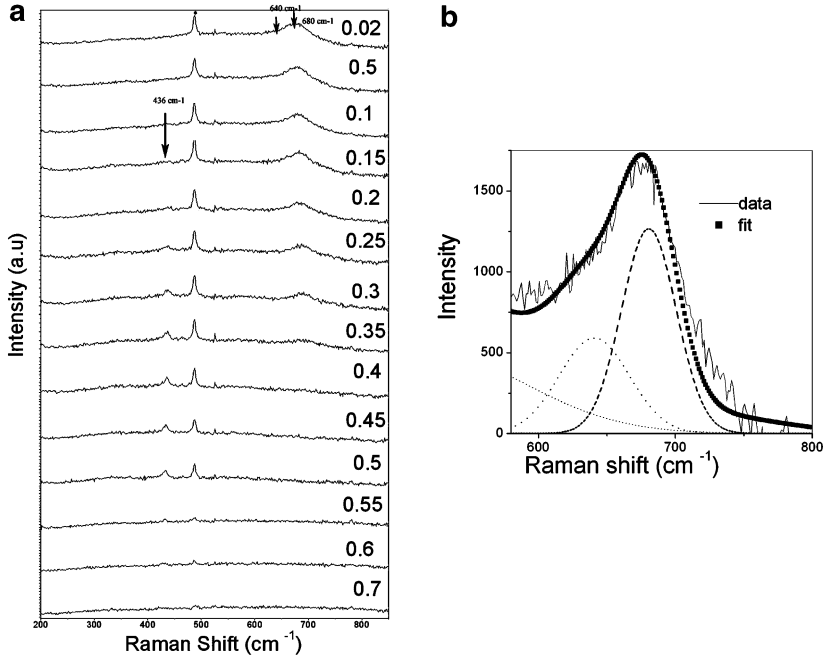

Figure 3. (a) Typical Raman spectra obtained at different compositions on the sample. The nominal Sr composition increase shown from top to bottom in the panel is derived from the X-ray data. The asterisk (*) represents the first-order Raman peak due to LAO substrate. (b) Resolving of the peak at 680 cm^{-1} into its components at $x = 0.1$. Also observed in the Figure is a contribution from a lower-frequency mode at 520 cm^{-1}, well-known for this composition.

Alternately exposing half of the substrate to the plume for each target produces composition gradient. This can easily be extended to more than two targets to create a 2-D composition spread. The complete process has been automated. A KrF Excimer laser (248 nm) with an energy density of 1.5−2 mJ/cm^2 was used. The spread films were deposited on 10-mm-wide $LaAlO_3$ (1 0 0) (LAO) substrate at 790 °C in a flowing oxygen gas at a chamber pressure of 100 mTorr. After the deposition, the films were then annealed at the deposition temperature for 1 h in 1 atm O_2 pressure.

Results and Discussion

Crystallinity and the orientation of the films were characterized using a high-resolution four-circle X-ray diffractometer. The overall $\theta-2\theta$ scan showed (00l) orientation of the entire composition spread and found no impurities within the experimental error (5%). Figure 2 shows the contour map of the $\theta-2\theta$ scans at varying positions on the film that were carried out using a line source focused to 5 × 0.5 mm using cross slits. The (002) diffraction peak of the composition spread film moves to a higher 2θ position with increasing Sr content. This is consistent with the larger *c*-lattice parameter of LMO. The continuous variation of the out-of-parameter indicates the change in composition of the spread film. The inset of Figure 2 shows the *d* values measured at different positions, including the end members LMO and SMO, and the nominal composition (*x*) of the spread film is shown in the upper panel. The observed out-of-plane parameter values are larger than their bulk *c* parameter; this can be understood from the compressive stress on the film due to the smaller lattice parameter of the LAO substrate (3.789 Å).

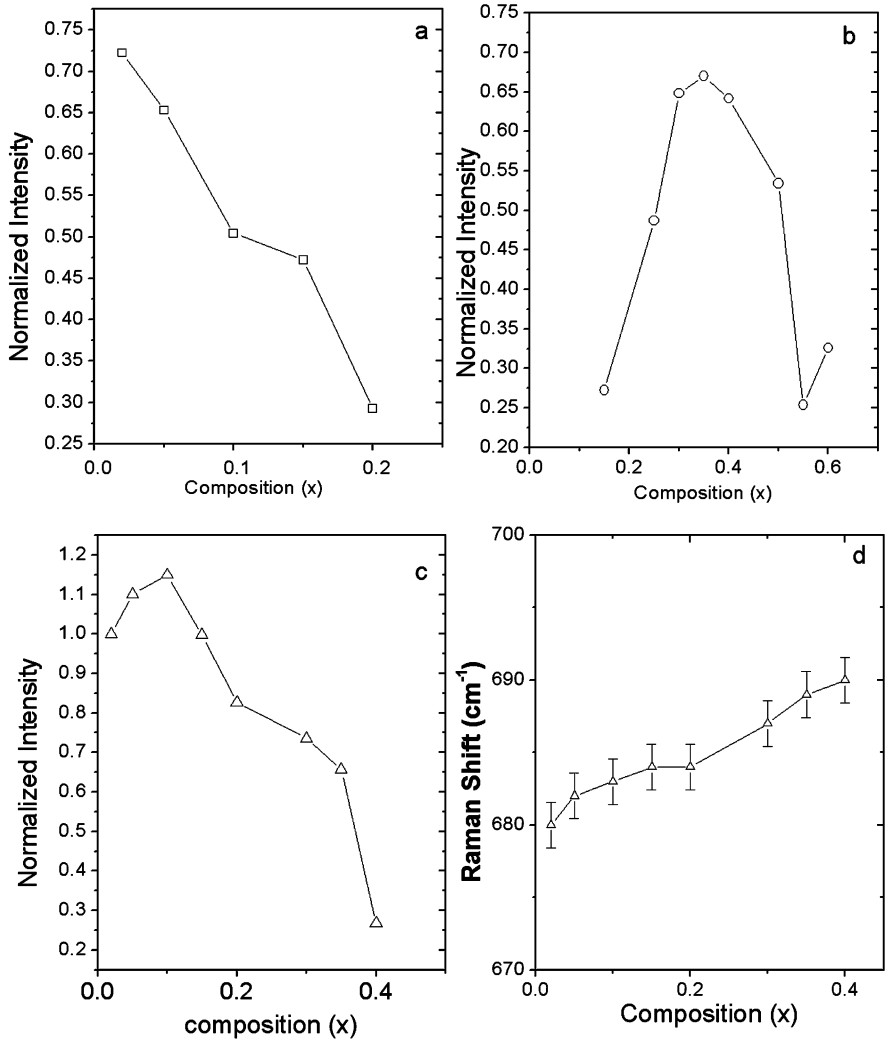

Figure 4. Normalized intensity versus composition plots for modes (a) 640, (b) 436, and (c) 680 cm^{-1} (d) shows the position of the 680 cm^{-1} mode versus composition.

The Raman study of the film was carried out in backscattering geometry using a Renishaw Ramanscope 1000 equipped with a CCD detector. An Ar ion laser with a 514.5-nm wavelength was focused at a 2-μm spot size on the sample. Raman spectra from the composition-spread LSMO sample were collected at different positions by scanning the laser spot along the sample surface. The Raman spectra were divided by the Bose−Einstein thermal factor $[1 - \exp(-\hbar\omega/k_B T)]$, where $\hbar$ is the Planks constant, ω is the mode frequency, k_B is the Boltzman constant, and T is the temperature at which the Raman spectra were recorded (300 K).[19] Spectra were recorded at variable laser power to ensure that there were no effects due to sample heating. Figure 3 shows the typical Raman spectra obtained at different compositions along the direction of the composition gradient (from La to Sr rich end). We observed peaks at 436 and 680 cm^{-1}. The peak at 680 cm^{-1} shows a clear shoulder feature around 640 cm^{-1}. This peak has been resolved into two peaks at 640 and 680 cm^{-1}, as shown in Figure 3b. Because all the spectra were collected under the same conditions in the same session, the spectra were normalized to the intensity of the 680 cm^{-1} mode at the LAO end. At the La-rich end, Raman spectra were dominated by the 640 and 680 cm^{-1} peaks; increasing Sr content initiates 436 cm^{-1} peak as shown in the Figure 3. A sharp peak at 525 cm^{-1} was not identified.

The Raman spectrum of orthorhombic LMO is dominated by two intense peaks at 500 and 610 cm^{-1} associated with the JT distortion.[10] For Sr doping, Raman spectra of LSMO with orthorhombic structure ($x < 0.17$) contain modes due to orthorhombic distortion similar to parent orthorhombic LMO. As the doping increases ($x > 0.17$), the symmetry of the structure changes to rhombohedral, characterized by the appearance of a mode at 436 cm^{-1}.[15,16] Recently, however, it has been shown that for oxygen-rich $LaMnO_{3+z}$, the case is more complicated.[11] Instead of sharp peaks at 500 and 610 cm^{-1}, the peaks are broader and shifted to 520 and 640 cm^{-1}; however, their attribution to a JT distortion mode for 520 and 640 cm^{-1} feature is kept. The positions of the 610 cm^{-1} peak increases in frequency as an increasing z in $LaMnO_{3+z}$.[12] On the basis of theses observations, the peaks observed on our films at 640 and 436 cm^{-1} were attributed to the JT effect and rhombohedral symmetry, respectively. The peak at 680 cm^{-1} will be discussed later.

The appearance and intensity variation of the peaks at 640 and 436 cm^{-1} moving along the direction of composition

gradient are shown in Figure 4a and b, respectively. The mode around 640 cm^{-1} decreases in intensity continuously as the Sr content increases. This is expected because the JT distortion decreases as Sr doping increases. Doping of Sr into LMO brings in a ferromagnetic metallic state from an antiferromagnetic insulating state. This transition is accompanied by a structural change from orthorhombic to rhombohedal with increasing Sr content. The Raman shifts are sensitive to the structural changes; the decrease in intensity of the 640 cm^{-1} mode is coincident with the appearance of the mode 436 cm^{-1} associated with the rhombohedral structure. It is interesting to note that for composition $x = 0.15$ on the sample, both 640 and 436 cm^{-1} modes are present, indicating the coexistence of the cooperative JT distortion with the rhombohedral structure. This is close to the phase coexistence predicted for LSMO single crystals at $x = 0.17$.[23] Above $x = 0.2$, the 640 cm^{-1} mode completely disappears. The intensity of the 436 cm^{-1} peak in Figure 4b shows a maximum at $x = 0.35$. It is worth mentioning that at $x = 0.33$, optimal doping and 100% spin polarization was observed in bulk crystals.[3] This peak disappears for $x > 0.6$, possibly indicating another structural change. No significant Raman peaks were observed for compositions above 0.6 on the sample. Previously, tetragonal structure was reported for Sr above 0.54 in LSMO;[22] however, the tolerance factor reaching close to 1.0 may lead to the cubic structure in the thin films that would be Raman-inactive and may explain the absence of Raman modes above 0.6. It is clear from the above observation that the intensity variation of the JT distortion, the appearance of the coexisting phases, and then the rhombohedral phase on the spread film are consistent with the structural and transport change observed in LSMO single crystals.[23]

Now we discuss the mode at 680 cm^{-1}. This mode has been neither predicted nor observed in orthorhombic LMO;[10] however, a lattice dynamical calculation on rhombohedral LMO shows a silent mode at 716 cm^{-1}.[11] A mode at 690 cm^{-1} has previously been observed in the LSMO thin films and single crystals.[13−15] The mode has variously been assigned to an impurity mode,[12] partial revealing of the phonon density of states (PDOS),[17] or as due to a second-order Raman scattering process.[12] A systematic variation of a peak at 710 cm^{-1} has been observed for Fe substitution of the Mn site in $La_{0.7}Sr_{0.3}MnO_3$.[20] Softening of this mode was observed as a consequence of an increase in the cell volume (or an increase in the Mn−O distance) due to Fe substitution. Recently, a mode at a similar Raman shift was observed in LMO single crystals for hydrostatic pressure above 7 kPa. Hardening of this mode is observed as increasing the pressure due to contracting Mn−O bonds.[18] The present Raman study on the continuous variation of $(La/Sr)MnO_3$ can give more insight on this mode. Figure 4c shows variation of the intensity of this mode as increasing Sr. We observed hardening of this mode as the Sr content increased from 680 to 690 cm^{-1} (for the compositions on the sample from $x = 0-0.4$ as in Figure 4 d). The intensity variation and the hardening of the mode rules out assigning this mode to an impurity. In the present case, deposition in the oxygen condition on a smaller lattice substrate can influence the Raman spectra. The deposition of the films in oxygen conditions can cause disorder from the formation of orthorhombic LMO. The disorder in LMO together with the compressive substrate strain can therefore either partially reveal the PDOS or activate the silent mode. The decrease of the lattice parameter from X-ray diffraction relates to the decrease in the Mn−O distance and is consistent with the hardening of this mode.

In conclusion, we prepared composition-gradient LSMO films by automated PLD at optimized deposition conditions. The reported method for obtaining the composite gradient is simple in a manner that does not involve complicated moving masks or prolonged annealing steps. Raman characterization showed modes due to structural changes and the coexistence of phases at the compositions expected for LSMO. The Raman results, therefore, complement the X-ray diffraction that showed a continuous change of the out-of-plane parameter with increasing Sr content. Raman spectra also give useful information about the effects due to disorder and strain. We anticipate that the Raman spectroscopy can be a rapid and nondestructive characterization technique for analyzing compositionally graded films to get an overview of the phase diagrams of complex systems that have varying phase boundaries and coexisting phases.

Acknowledgment. This work was funded by EPRSC.

References and Notes

(1) *Colossal Magnetoresistive Oxides*; Tokura, Y., Ed.; Advances in Condensed Matter Science; Gordon and Breach Science Publishers: Amsterdam, 2000; Volume 2.
(2) Millis, J.; Littlewood, P. B.; Shraiman, B. I. *Phys. Rev. Lett*. **1995**, *74*, 5144−5147.
(3) Park, J.-H.; Vescovo, E.; Kim, H.-J.; Kwon, C.; Ramesh, R.; Venkatesan, T. *Nature* **1998**, *392*, 794.
(4) Brice, g.; Chang, H.; Sun, X.; Schultz, P. G.; Xiang, X.-D. *Science* **1995**, *270*, 273.
(5) Yoo, Y. K.; Duewer, F.; Fukumura, T.; Yang, H.; Yi, D.; Liu, S.; Chang, H.; Hasegawa, T.; Kawasaki, M.; Koinuma, H.; Xiao-Dong, X. *Phys. Rev. B: Condens. Matter Mater. Phys.* **2001**, *63*, 224421.
(6) Güttler, B.; Gorbenko, O. Yu.; Novozhilov, M. A.; Samoylenkov, S. V.; Amelitchev, V. A.; Wahl, G.; Zandbergen, H. W. *J. Phys. IV* **1999**, *9*, 1179.
(7) Fukumura, T.; Ohtani, M.; Kawasaki, M.; Okimoto, Y.; Kageyama, T.; Koida, T.; Hasegawa, T.; Tokura, Y.; Koinuma, H. *Appl. Phys. Lett*. **2002**, *77*, 3426.
(8) Gibson, G.; MacManus-Driscoll, J. L.; Cohen, L. F. *IEEE Trans. Appl. Supercond.* **1997**, *7*, 2130.
(9) Quilty, J. W.; Trodahl, H. J. *Phys. Rev. B: Condens. Matter Mater. Phys.* **2000**, *61*, 4238.
(10) Iliev, M. N.; Abrashev, M. V.; Lee, H.-G.; Popov, V. N.; Sun, Y. Y.; Thomsen, C.; Meng, R. L.; Chu, C. W. *Phys. Rev. B: Condens. Matter Mater. Phys.* **1998**, *57*, 2872.
(11) Abrashev, M. V.; Litvinchuk, A. P.; Iliev, M. N.; Meng, R. L.; Popov, V. N.; Ivanov, V. G.; Chakalov, R. A.; Thomsen, C. *Phys. Rev. B: Condens. Matter Mater. Phys.* **1999**, *59*, 4146.
(12) Granado, E.; García, A.; Sanjurjo, J. A.; Rettori, C.; Torriani, I.; Prado, F.; Sánchez, R. D.; Caneiro, A.; Oseroff, S. B.

Phys. Rev. B: Condens. Matter Mater. Phys. **1999**, *60*, 11879.
(13) Bormann, D.; Desfeux, R.; Degave, F.; Khelifa, B.; Hamet, J. F.; Wolfman, J. *Phys. Status Solidi B* **1999**, *215*, 691.
(14) Dediu, V. A.; López, J.; Matacotta, F. C.; Nozar, P.; Ruani, G.; Zamboni, R.; Taliani, C. *Phys. Status Solidi B* **1999**, *215*, 625.
(15) Podobedov, V. B.; Weber, A.; Romero, D. B.; Rice, J. P.; Drew, H. D. *Solid State Commun*. **1998**, *105*, 589.
(16) Podobedov, V. B.; Weber, A.; Romero, D. B.; Rice, J. P.; Drew, H. D. *Phys. Rev. B: Condens. Matter Mater. Phys.* **1998**, *58*, 43.
(17) Iliev, M. N.; Abrashev, M. V.; Popov, V. N.; Hadjiev, V. G. *Phys. Rev. B: Condens. Matter Mater. Phys.* **2003**, *67*, 212301.
(18) Loa, I.; Adler, P.; Grzechnik, A.; Syassen, K.; Schwarz, U.; Hanfland, M.; Rozenberg, G. Kh.; Gorodetsky, P.; Pasternak, M. P. *Phys. Rev. Lett*. **2001**, *87*, 125501.
(19) Yoon, S.; Liu, H. L.; Schollerer, G.; Cooper, S. L.; Han, P. D.; Payne, D. A.; Cheong, S. W.; Fisk, Z. *Phys. Rev. B: Condens. Matter Mater. Phys.* **1998**, *58*, 2795.
(20) Souza Filho, A. G.; Faria, J. L. B.; Guedes, I.; Sasaki, J. M.; Freire, P. T. C.; Freire, V. N.; Mendes Filho, J.; Xavier, M. N., Jr.; Cabral, F. A. O.; de Araújo, J. H.; da Costa, J. A. P. *Phys. Rev. B: Condens. Matter Mater. Phys.* **2003**, *67*, 052405.
(21) Christen, H. M.; Silliman, S. D.; Harshavardhan, K. S. *Appl. Surface Sci*. **2002**, *189*, 216.
(22) Moritomo, Y.; Akimoto, T.; Nakamura, A.; Ohoyama, K.; Ohashi, M. *Phys. Rev. B: Condens. Matter Mater. Phys.* **1998**, *58*, 5544−5549.
(23) Urushibara, A.; Moritomo, Y.; Arima, T.; Asamitsu, A.; Kido, G.; Tokura, Y. *Phys. Rev. B: Condens. Matter Mater. Phys.* **1995**, *51*, 14103.

CC049927B